Structure and Reaction Geometry of Geranylgeranyl Diphosphate Synthase from *Sinapis alba*[†,‡]

Daniel P. Kloer,[§] Ralf Welsch,[||] Peter Beyer,[||] and Georg E. Schulz*[,§]

Institut für Organische Chemie und Biochemie, Albert-Ludwigs-Universität, Albertstrasse 21, D-79104 Freiburg im Breisgau, Germany, and Institut für Biologie II, Albert-Ludwigs-Universität, Schänzlestrasse 1, 79104 Freiburg im Breisgau, Germany

Received August 3, 2006; Revised Manuscript Received October 10, 2006

ABSTRACT: The crystal structure of the geranylgeranyl diphosphate synthase from *Sinapis alba* (mustard) has been solved in two crystal forms at 1.8 and 2.0 Å resolutions. In one of these forms, the dimeric enzyme binds one molecule of the final product geranylgeranyl diphosphate in one subunit. The chainfold of the enzyme corresponds to that of other members of the farnesyl diphosphate synthase family. Whereas the binding modes of the two substrates dimethylallyl diphosphate and isopentenyl diphosphate at the allyl and isopentenyl sites, respectively, have been established with other members of the family, the complex structure presented reveals for the first time the binding mode of a reaction product at the isopentenyl site. The binding geometry of substrates and product in conjunction with the protein environment and the established chemistry of the reaction provide a clear picture of the reaction steps and atom displacements. Moreover, a comparison with a ligated homologous structure outlined an appreciable induced fit: helix α8 and its environment undergo a large conformational change when either the substrate dimethylallyl diphosphate or an analogue is bound to the allyl site; only a minor conformational change occurs when the other substrate isopentenyl diphosphate or the product is bound to the isopentenyl site.

As geranylgeranyl diphosphate (GGPP)[1] contains isoprene units, it belongs to the large and diverse group of isoprenoids. The biosynthesis of isoprenoids starts with the formation of a linear oligomer or polymer. Subsequently, a virtually unlimited number of modifications are introduced by cyclization, oxidation/reduction, cleavage, and group transfer (*1*). An important linear isoprenoid is the C_{20} compound geranylgeranyl diphosphate (GGPP), which is involved in several biosynthetic routes. For example, it may be added to non-prenyl acceptors to form chlorophyll or α-tocepherol (*2*), cyclized to result in *ent*-kaurene or taxadiene (*3*), or directly used for protein prenylation (*4*). Also, two GGPP molecules may undergo a head-to-head condensation to form phytoene. Phytoene is then desaturated and modified with oxygen functions, giving rise to numerous carotenoids, some of which are degraded to yield apo-carotenoids, such as retinal (*5*).

In isoprenoid biosynthesis, the basic units are isopentenyl diphosphate (IPP), which is synthesized in the mevalonate or methylerythritol phosphate pathways, depending on the organism and subcellular location (*6*, *7*) and its isomer dimethylallyl diphosphate (DMAPP), required as a starter molecule. The condensation of DMAPP with IPP is catalyzed by enzymes such as GGPP synthase, releasing the diphosphate of DMAPP. The resulting geranyl diphosphate possesses the allylic arrangement required for the addition of another IPP molecule so that, in principle, the process can be repeated indefinitely (Figure 1). A given synthase usually catalyzes several subsequent steps until a final product length is reached. The presence of Mg^{2+} or Mn^{2+} ions is generally required (*8*). Here, we focus on farnesyl diphosphate (FPP) and GGPP synthases, because structures of bound substrates and analogues are known for these enzymes. Note that the addition of IPP occurs generally in trans with respect to the newly formed double bond, although cis additions are also known (*9*−*11*).

All enzymes catalyzing the trans addition belong to a single family, which was first characterized by two aspartate-rich motifs with the consensus sequences DDx--xD (x indicates any residue and the dashes a two-residue insertion in some family members) and DDxxD, respectively (*12*). Because the first crystal structure of a family member was that of an FPP synthase (*13*), we propose the name "FPP synthase family". FPP and GGPP synthases as well as family members synthesizing longer chains (*14*, *15*) are generally homodimers with symmetry axes at equivalent positions. However, human GGPP synthase forms trimers of these dimers, i.e., hexamers (*16*), and heterodimers are known for some long-chain synthases (*17*). Here, we report the crystal structure of the GGPP synthase from the plant *S. alba*, outlining induced-fit movements around the binding sites and

[†] This work was supported by the Deutsche Forschungsgemeinschaft under grant SFB-388.

[‡] The atomic coordinates and structure factors have been deposited in the Protein Data Bank as 2J1O and 2J1P.

* Corresponding author. Telephone: +49-761-203-6058. Fax: +49-761-203-6161. E-mail: georg.schulz@ocbc.uni-freiburg.de.

[§] Institut für Organische Chemie und Biochemie.

[||] Institut für Biologie II.

[1] Abbreviations: DMAPP, dimethylallyl diphosphate; FPP, farnesyl diphosphate; GGPP, geranylgeranyl diphosphate; IPP, isopentenyl diphosphate; MAD, multiwavelength anomalous diffraction; SeMet, seleno−methionine.

10.1021/bi061572k CCC: $33.50
Published on Web 12/01/2006

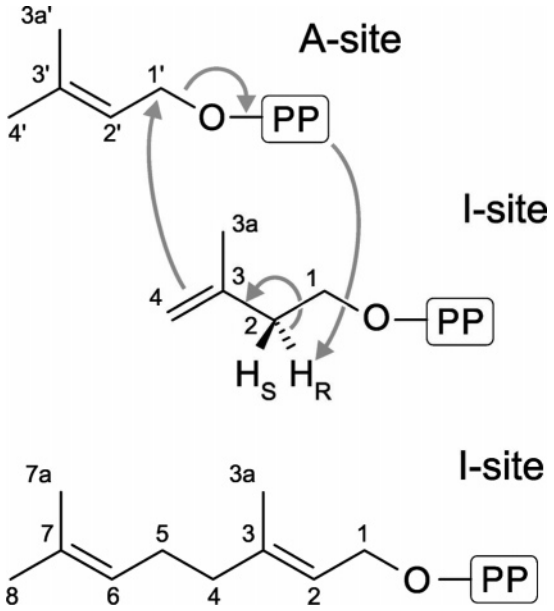

FIGURE 1: Sketch of the condensation reaction of IPP at the isopentenyl or I-site and DMAPP at the allyl or A-site, yielding geranyl diphosphate at the I-site. The reaction starts with the generation of an allylic cation at the A-site and runs in a circle, as indicated. The diphosphate of DMAPP with the 2-H_R proton of IPP is released (*41*). The newly formed C2−C3 double bond is trans. For further steps, the diphosphate of the product has to move from the I- to the A-site and a new IPP molecule has to occupy the I-site.

revealing the binding mode of the reaction product, which completes our knowledge of the reaction geometry.

MATERIALS AND METHODS

Expression and Purification of GGPP Synthase. The cDNA of the GGPP synthase from *S. alba* was obtained as described (*18*) and inserted into vector pQE30 (Qiagen) to be expressed in *Escherichia coli* BL21(DE3) cells (Novagen). A single colony was used to inoculate a 37 °C overnight culture of 15 mL of Luria−Bertani (LB) medium with 150 μg/mL ampicillin. The cells were centrifuged, resuspended in 400 mL of LB medium (150 μg/mL ampicillin), grown at 37 °C to an OD_{600} of 0.7, supplemented with 0.1 mM isopropylthiogalactoside (IPTG), incubated for 4 h, and then harvested by centrifugation and frozen at −20 °C.

Frozen cells were resuspended in buffer A (10 mM sodium phosphate pH 7.9, 5 mM β-mercaptoethanol), sonicated, and centrifuged. The supernatant was applied to an anion exchange column (Resource Q, Pharmacia) equilibrated with buffer A and eluted with a 0−1 M NaCl gradient in buffer A. Fractions containing GGPP synthase were loaded onto a Talon Co^{2+} column (ClonTech, Heidelberg) equilibrated with buffer B (20 mM sodium phosphate pH 7.4, 20 mM imidazole, 500 mM NaCl, 5 mM β-mercaptoethanol). After washing with buffer B, the protein was eluted with a 0−500 mM imidazole gradient in buffer B. GGPP synthase was then concentrated to 10−20 mg/mL and run through a gel permeation column (Superdex S200 16/60, Pharmacia) equilibrated with buffer C (20 mM Tris−HCl pH 7.9, 200 mM NaCl, 2 mM EDTA, 2 mM DTT), resulting in a single peak. Seleno-methionine (SeMet) was incorporated using the pathway inhibition method (*19*). All subsequent purification steps were carried out as described for the native enzyme.

Table 1: Structure Analysis

	SeMet-labeled GGPP synthase[b]			native GGPP synthase[c]
data collection[a]	inflection	peak	remote	
wavelength (Å)	0.97967	0.97943	0.97701	0.98243
resolution (Å)	34 − 1.8	38 − 1.8	31 − 1.8	50 − 2.0
unique reflections	94523	94447	95260	26607
multiplicity	2.0	2.0	1.9	8.5
completeness (%)	95.6 (91.5)	95.5 (91.6)	96.4 (94.9)	99.1 (96.5)
R_{sym} (%)	4.1 (48)	4.1 (47)	4.3 (46)	6.5 (31)
I/σ_I	10.6 (1.6)	10.4 (1.7)	10.5 (1.8)	17.2 (5.5)
Wilson *B*-factor (Å^2)	26	27	27	39

	SeMet-labeled GGPP synthase[b]	native GGPP synthase[c]
refinement	remote	
number of protein atoms	4173[d]	1895[e]
number of ligand atoms	47	
number of solvent atoms	190	89
R_{cryst}/R_{free}(%)	17.0 / 20.9	19.6 / 22.9
average *B*-factors (Å^2)		
mainchain (subunit A/B)	38 / 32	46
side-chains (subunit A/B)	39 / 36	52
ligand GGPP (subunit A)	41	
water molecules	42	46
rmsd bond lengths (Å)/angles (deg)	0.019 / 1.67	0.018 / 1.52
Ramachandran (%): favored/allowed	98.3 / 1.7	98.4 / 1.6

[a] All reported data were collected at beamline X06SA of the SLS (Villigen, Switzerland). [b] The crystal belonged to space group $P2_1$ with unit cell parameters $a = 53.8$ Å, $b = 91.5$ Å, $c = 56.3$ Å, and $\beta = 97.0°$ with 2 subunits per asymmetric unit. The pH is 4.4. The solvent content is 41%. [c] The crystal belonged to space group $P3_121$ with unit cell axes $a = b = 71.8$ Å, $c = 127.9$ Å with 1 subunit per asymmetric unit. The pH is 10.0. The solvent content is 57%. [d] Residues 72−230, 234−299, 316−366 of subunit A and 71−301, 316−361 of subunit B. [e] Residues 72−152, 171−230, 238−298, and 313−363.

Crystallization and Structure Elucidation. For crystallization, GGPP synthase was concentrated to 20 mg/mL and dialyzed against 10 mM Tris-HCl pH 7.9, 10 mM $MgCl_2$, 100 mM NaCl, 0.5 mM tris(2-carboxyethyl)phosphine (TCEP). Crystals of SeMet-labeled GGPP synthase were obtained by vapor diffusion with hanging drops that contained a 1:1 mixture of protein solution and reservoir buffer D (100 mM sodium acetate pH 4.4, 40% (v/v) propanediol, 10 mM $MgCl_2$, 0.5 mM TCEP). They were frozen in liquid nitrogen without the addition of a cryo protectant. A second crystal form was obtained with native GGPP synthase using the same procedure but with reservoir buffer E (100 mM *N*-cyclohexyl-3-aminopropane sulfonic acid (CAPS) pH 10.0, 200 mM NaCl, 9−11% PEG 8000, 10 mM $MgCl_2$, 0.5 mM TCEP). These crystals were transferred in six steps into reservoir buffer E containing 30% (v/v) glycerol and then flash-frozen in liquid nitrogen.

Multiwavelength anomalous diffraction (MAD) data sets of SeMet-labeled GGPP synthase and a data set of the native enzyme were collected at 100 K at the Swiss Light Source (Villigen, Switzerland) (Table 1). All data were processed with XDS and XSCALE (*20*). The selenium positions were located with SHELXD (*21*) and used for phasing with SHARP (*22*). After solvent flattening, histogram matching, and noncrystallographic symmetry averaging with RESOLVE (*23*), the maps allowed model building with ARP/wARP (*24*). The model was improved using XFIT (*25*) and refined with BUSTER (*26*, *27*) and REFMAC5 (*28*) (Table 1). During the course of refinement, difference maps revealed

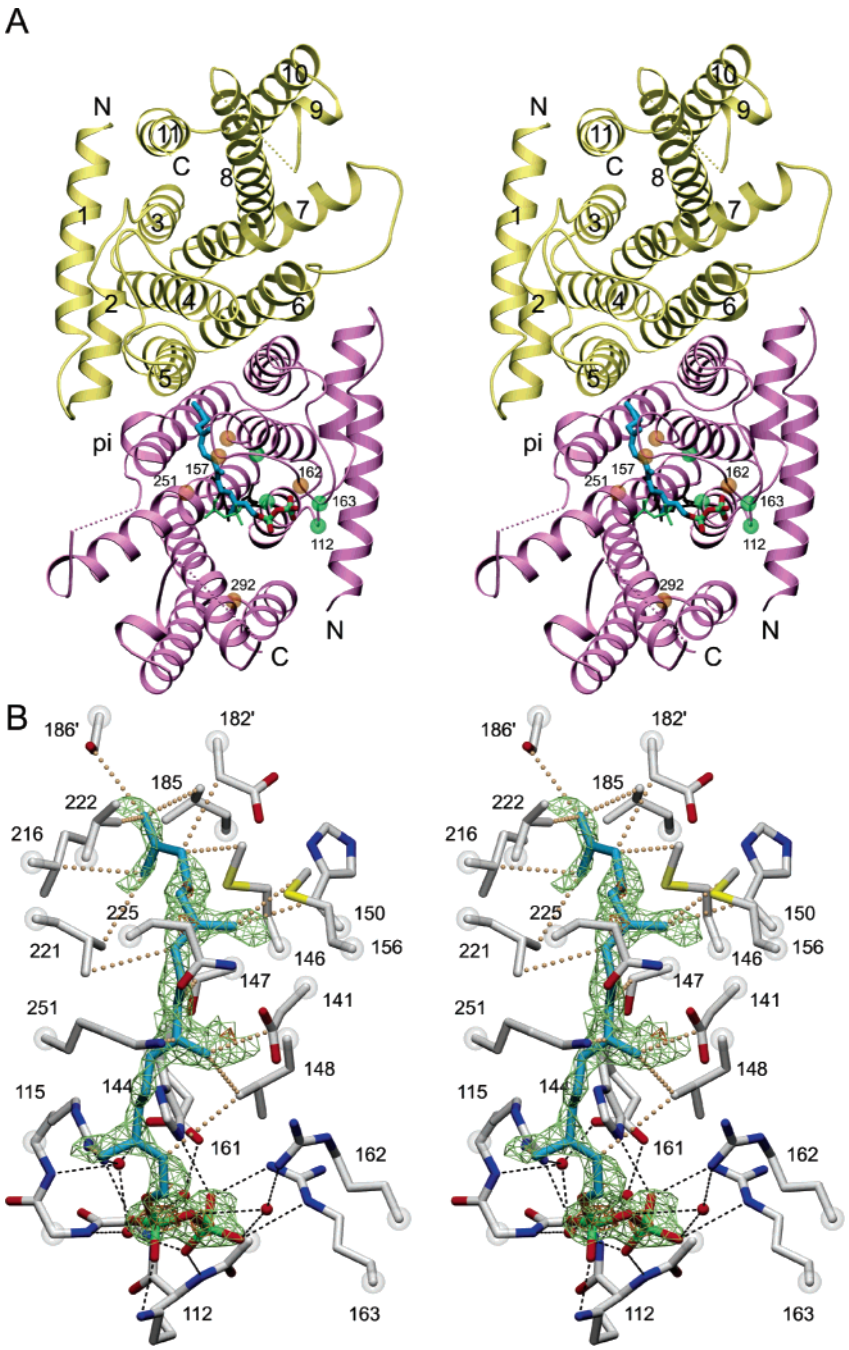

FIGURE 2: Structure of GGPP synthase from *S. alba*. (A) Stereoview of a ribbon plot of the GGPP synthase dimer in the $P2_1$ crystals (Table 1), showing chain A with the bound GGPP molecule at the bottom. The residues participating in the A- and I-sites are indicated by orange and green transparent spheres, respectively, in correspondence with Figure 3. The α-helices of chain B are numbered sequentially. The π-bulge at the interface is labeled. Unstructured chain segments are indicated by straight dotted lines. The inhibitory binding mode of GGPP at human GGPP synthase (*16*) is shown as a thin stick model (diphosphate green, isoprenyls black). The position of this GGPP molecule was derived from a backbone alignment with the homologous human enzyme. (B) Stereoview of the GGPP molecule bound to the I-site within the surrounding residues. Hydrogen bonds are indicated by black dashed lines, and van der Waals contacts with distances of less than 4.5 Å are orange dotted lines. The two methionines contain selenium instead of sulfur atoms. The initial $(F_o - F_c)$-difference electron density of GGPP is shown at 2.5 and 4.0σ levels. The GGPP site is fully occupied. After the refinement, the $(2F_o - F_c)$-electron density clearly outlined all non-hydrogen atoms of GGPP at the 1.4σ level, confirming the interpretation.

the presence of the reaction product GGPP in subunit A of the SeMet-labeled crystal, which was then modeled using PRODRG2 (*29*). The structure of native GGPP synthase (Table 1) was solved independently using the single isomorphous replacement anomalous scattering method with a xenon derivative (data not shown) and improved with RESOLVE (*23*). An initial model built with ARP/wARP was completed and refined as described above (Table 1).

RESULTS AND DISCUSSION

Structure Determination. The cDNA of GGPP synthase from the plant *S. alba* was expressed in *E. coli* at a medium level in order to keep the enzyme in the cytosolic fraction. An N-terminal His_6-tag was used for purification. The yield was about 15 mg of pure enzyme per liter culture. The analyzed GGPP synthase construct consisted of 304 residues (at positions 63−366) with a mass of 33 kDa. Consistently,

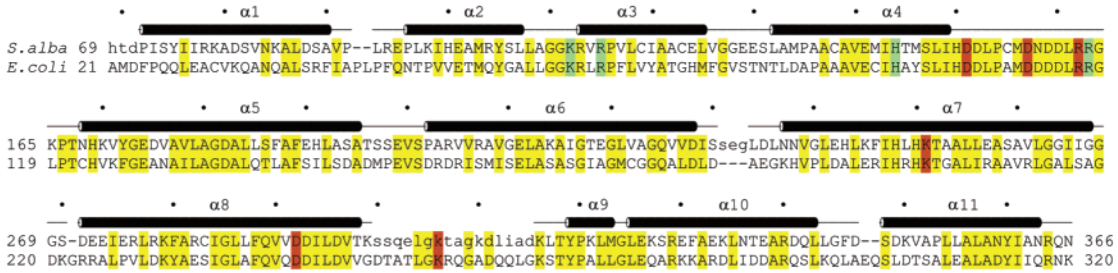

FIGURE 3: Structure-based sequence alignment of the GGPP synthase from *S. alba* with the FPP synthase from *E. coli* (*33*). Lowercase letters indicate disordered structures. The *S. alba* sequence numbers include a signal peptide of about 60 residues. The applied construct starts at position 63 with a His_6-tag, and the native sequence starts at position 74. The secondary structure and the marks (·) are for the *S. alba* enzyme. The *E. coli* sequence starts with the structured part. The residues contacting the diphosphate of the A-site either directly or via Mg^{2+} are orange. They comprise the two DDxxD motifs. The residues contacting the diphosphate of the I-site are green.

Table 2: Observed Substrate Binding Positions in Enzymes of the FPP Synthase Family

protein	source	allyl- or A-site	isopentenyl- or I-site	isoprenyl pocket	reference
FPP synthase[a]	*Gallus gallus*	FPP[a]		+[a]	35
FPP synthase	*Escherichia coli*	DMAPP			
		DMSPP[b]	IPP		33
		risedronate	IPP		33
FPP synthase	*Homo sapiens*	risedronate[c]			39, 40
		zoledronate	IPP		39, 40
FPP synthase	*Trypanosoma cruzi*	risedronate	*d*		42
		alendronate	IPP		42
GGPP synthase[e]	*Homo sapiens*	GGPP[e]		other[e]	16
GGPP synthase	*Sinapis alba*		GGPP	+	this paper

[a] The authors report FPP binding to a mutant with an elongated isoprenyl pocket that synthesizes GGPP. [b] DMSPP is the 1-thio analogue of DMAPP. [c] In addition, ref 40 reports complexes with pamidronate, ibandronate, and alendronate. [d] The authors claim to observe a DMAPP molecule near this site but provide an inconsistent model. [e] Whereas all other proteins are dimers, this is a trimer of these dimers, i.e., a hexamer. The geranylgeranyl moiety of GGPP does not bind in the common chain pocket but at a special site occluding the I-site and thus inhibiting the enzyme.

the gel permeation runs showed a single peak at 67 kDa, corresponding to a dimer. Screenings with native GGPP synthase resulted in crystals that grew at pH 10.0 over 3 days to sizes of 400 × 100 × 100 μm^3 and belonged to the space group $P3_121$ with one subunit in the asymmetric unit.

For phasing, the enzyme was SeMet-labeled using the pathway inhibition method (*19*) and purified like the native protein. The yield was about 9 mg of protein per liter culture. Screenings resulted in crystals that grew at pH 4.4 over 10 days to sizes of 300 × 50 × 30 μm^3 and belonged to the space group $P2_1$ with a dimer in the asymmetric unit. MAD data revealed two sets of six selenium sites related by a local 2-fold axis, which was in good agreement with the six methionines of the amino acid sequence. MAD phasing, density improvement, and refinement yielded a model of good quality (Table 1).

The structure of the native enzyme was established parallel to the SeMet-labeled enzyme using a xenon derivative for phasing. The resulting model of native GGPP synthase (Table 1) confirmed that of the SeMet-labeled enzyme. The refinement of the native enzyme showed no bound ligand. Experiments involving cocrystallization and soaking the native enzyme with FPP and Mg^{2+} failed. However, phasing and refinement of the SeMet-labeled GGPP synthase revealed a GGPP molecule bound to chain A at 100% occupancy but no ligand bound in the corresponding pocket of chain B. Such an asymmetric ligand binding to a homodimer with noncrystallographic symmetry is not exceptional because the packing contacts may introduce enough asymmetry (*30*).

The structure of the enzyme−product complex is depicted in Figure 2. A comparison between native and SeMet-labeled GGPP synthase showed no significant structural difference, although small variations occurred in regions of high mobility, especially at crystal packing contacts. The bound GGPP was clearly identified by the electron density (Figure 2B). It caused only minor conformational changes. Most likely, this GGPP molecule was picked up from the *E. coli* cytosol and kept during purification and crystallization. Possibly, the replacement of the sulfurs of Met146 and Met156 by selenium increased the affinity of the binding site (Figure 2B). It is also conceivable that the applied pathway inhibition method for SeMet-labeling (*19*) or the large amount of the produced GGPP synthase enhanced the GGPP concentration in *E. coli* during protein expression. Such a retaining of a metabolite during protein purification and crystallization is rare, but other cases are known (*31*, *32*).

The polypeptide of GGPP synthase is organized in eleven α-helices, like all other members of the FPP synthase family. Along the chain, the mobility is generally low in the α-helices but high in the connections between them. Some of these connections were so mobile that the chain could not be localized because of the lack of density (Table 1). The two independent subunits A and B in the SeMet-labeled crystals showed different mobilities. This asymmetry is caused by different crystal contacts and may explain why GGPP was only bound to subunit A.

As illustrated in Figure 2A, GGPP synthase contains a large active center pocket that is elongated toward the dimer interface in order to accommodate the C_{20} product GGPP. The substrate binding pockets of the two subunits reach the interface but do not meet there, so that in principle both active centers may work independently. The interface buries a solvent accessible area of 1600 $Å^2$ of each subunit; it is enlarged by a π-bulge in helix α6. This π-bulge consists of the sequence -GTEG-, where the glycines assume glycine-specific torsion angles. Such a π-bulge is also present in the dimeric FPP synthase from *E. coli* (*33*) but missing in the hexameric GGPP synthase from *Homo sapiens* (*16*).

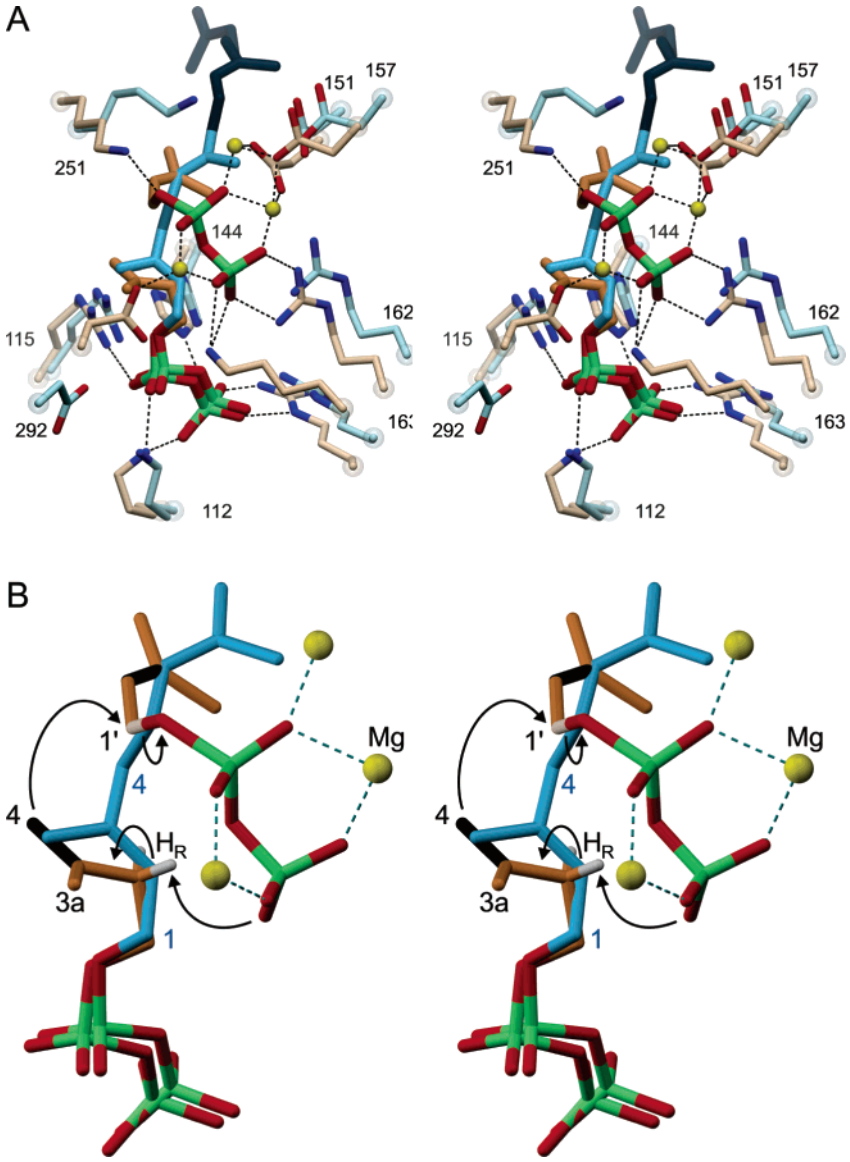

FIGURE 4: Stereoview of the isoprenoid elongation reaction sketched in Figure 1. (A) Substrates DMAPP and IPP bound to the FPP synthase from *E. coli* (orange) (*33*) superimposed on the final product GGPP bound to the enzyme from *S. alba* (blue). The DMAPP position corresponds to that of its 1-thio analogue DMSPP (Table 2). Important active center residues of the *E. coli* and *S. alba* enzymes are beige and blue, respectively. The numbers are for the *S. alba* enzyme. In the *S. alba* enzyme, the A-site is not occupied. The lysine in front, binding to the diphosphate at the A-site, corresponds to the unstructured Lys306 of the *S. alba* enzyme, which probably adopts a defined structure only on A-site occupation. The initially synthesized half of GGPP is shaded dark blue. (B) Stereochemistry of the reaction as excerpted from panel A, showing the A-site with DMAPP at the top and the I-site with IPP at the bottom. Double bonds are black. The final product GGPP found in the *S. alba* enzyme is truncated to the actual product of the depicted reaction (blue), which is geranyl diphosphate (Figure 1). Electron attacks are indicated by curved black arrows. The displacement of the C4 atom of IPP is 2.5 Å to the new position 4 (blue) of the product geranyl diphosphate.

Comparison with Related Structures. A search through the Protein Data Bank using DALI (*34*) revealed the FPP synthase from *E. coli* (*33*) as the closest structurally known relative of the reported GGPP synthase. A structure-based alignment showed 39% sequence identity between these two enzymes (Figure 3). More distantly related enzymes are the FPP synthase from *Gallus gallus* (*35*) and enzymes from *Sulfolobus solfataricus* (*14*) and *Thermotoga maritima* (*15*) producing linear hexa- and octa-isoprenyl diphosphate, respectively. Other GGPP synthases are structurally known (*16*, *36*), but they are not very closely related. The sequence identities are generally below 20%, indicating a significant evolutionary drift in this family.

All family members catalyze essentially the same reaction, namely the synthesis of linear isoprenoids in trans-configuration by a sequential addition of IPP molecules. Catalytically similar enzymes that add IPP in cis instead of trans configuration have completely different chainfolds (*9*−*11*) and are not further discussed here. With respect to the chainfold and also with respect to the DDxxD motifs, the FPP synthase family also comprises more distantly related enzymes that cyclize linear isoprenoids, such as the aristolochene synthase (*37*), or fuse them to head-to-head compounds, such as squalene synthase (*38*); these are not discussed here.

Recently, FPP synthases were identified as the target of nitrogen-containing bisphosphonate drugs used in the treatment of osteoporosis and related diseases (*39*, *40*). This observation initiated quite a number of structure analyses. Because we are mostly interested in the reaction geometry, we have restricted the comparison to the structures of

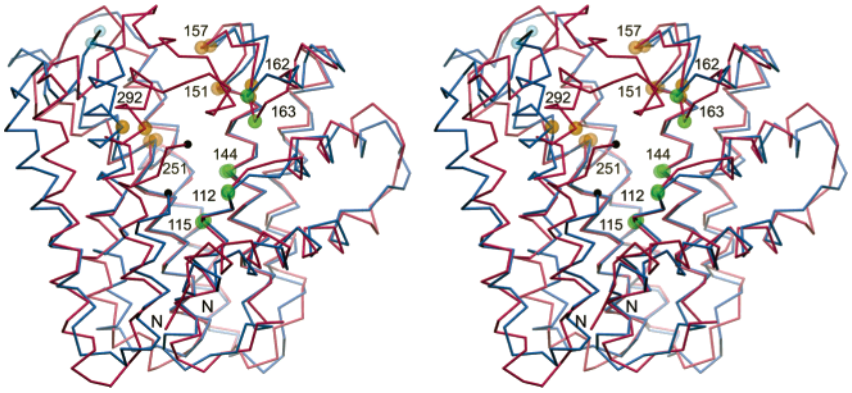

FIGURE 5: Superposition of the Cα backbone plots of GGPP synthase from *S. alba* chain B without ligand (blue) with that of FPP synthase from *E. coli* with the bound ligands IPP and DMSPP (red) (*33*). The important residues of the A- and I-sites are marked as in Figures 2A and 3. The unstructured segment 302−315 of the *S. alba* enzyme is indicated by a black line between the two blue transparent spheres. This segment adopts its native structure when the A-site is occupied. Note the rather extensive induced fit on DMAPP binding to the A-site and the comparatively small changes at the I-site on IPP binding.

enzyme−ligand complexes, all of which are listed in Table 2.

Geometry of the Catalyzed Reaction. The reaction catalyzed by the members of the FPP synthase family is depicted in Figure 1. Chemical studies showed that the C4 atom of IPP is connected to the C1′ atom of DMAPP and that the diphosphate of DMAPP and the H_R proton at the C2 atom of IPP are released (*9*, *12*, *41*). The enzymes have two physically distinct binding sites, anchoring the diphosphates of the two substrates, which we suggest naming "allyl" or "A-site" and "isopentenyl" or "I-site". During the reaction, IPP is elongated and remains bound to the I-site. For a further chain elongation, the diphosphate moiety of the product has to move from the I- to the A-site, and the next IPP molecule has to occupy the I-site (Figure 4).

The initial structure analysis of an FPP synthase showed two rather distant locations of the two DDxxD motifs, each with a bound metal ion (*13*), suggesting that they constitute the two binding sites of the diphosphates of the two substrates DMAPP and IPP. This interpretation prevailed for several years (*15*, *35*) until a complex structure (*33*) showed that both DDxxD motifs together with three Mg^{2+} ions form the A-site, whereas the I-site does not contain a metal ion but only positively charged amino acid side-chains (Table 2). In hindsight, such a difference was to be expected because the production of the allylic cation requires a very strong polarization, which is achieved by the three Mg^{2+} ions contacting the diphosphate oxygens at the A-site, whereas the diphosphate of IPP merely has to be bound and not polarized. In contrast to the other presently known structures, the *S. alba* enzyme binds the final product GGPP to the I-site (Figure 2B) rather than to the A-site (Table 2).

In Figure 4A, we have superimposed the structure of a DMAPP analogue and IPP bound to the FPP synthase from *E. coli* (*33*) with the reported GGPP complex of chain A. This shows the positions of the two substrates and of the final product GGPP. For clarification, the DMAPP analogue and IPP as well as the product geranyl diphosphate (the respective part of GGPP) are excerpted into Figure 4B. The double bond of IPP was assigned according to the protein environment, as it brings the π-electrons close to Arg115-Nη1 and away from the oxygens of Asp292 of the DDxxD motif. The reaction starts with the removal of the diphosphate of DMAPP, leaving an allylic carbocation, which is attacked by the C−C double bonds of IPP (Figures 1 and 4). The C1′ of DMAPP is the best suited target for the attack. The only available base for picking up the H_R proton is an oxygen of the DMAPP diphosphate (*37*), so that the reaction runs in a circle, as indicated in Figure 4B. The position of the product shows that, during the reaction, the C4 and the C3′ atoms move by 2.5 and 1.5 Å, respectively. The geometry excludes a cis elongation.

All nitrogen-containing bisphosphonate drugs were bound to the A-site and, in most structures, the I-site was occupied by the substate IPP (Table 2). Only in the structure reported here did the I-site accommodate the final reaction product GGPP (Figure 2B). Interestingly, in the GGPP synthase from *H. sapiens* (*16*), the product molecule GGPP was bound to the A-site extending into a pocket specific to this enzyme (Figure 2A) so that it occludes the I-site, suggesting a product inhibition (*16*). Because GGPP is the final product of this enzyme it cannot bind with its diphosphate to the A-site and at the same time extend its carbon chain into the common isoprenyl pocket.

Induced Fit. In our structure analysis, we found high mobility at the N- and C-termini, as well as around positions 233 and 305 near the A-site (Figure 2A). In contrast, the related structures with an occupied A-site (Table 2) showed continuous electron density in these segments. Actually, segment 300−315 backed up by segment 231−233 closes like a lid on the A-site, shielding it from the solvent during the reaction (Figure 5). The closure implies, however, that the segment opens up again in order to release the diphosphate from the A-site after the reaction, explaining its mobility. The solvent-excluding conformational change on A-site occupation is consistent with the observation that A-site binding is entropy-driven (*39*). The superposition of Figure 5 shows a classical induced fit on substrate binding to the A-site. A closer inspection reveals that, in addition, the structured polypeptide around the second DDxxD motif shifts by up to 5 Å. As a consequence, the two DDxxD motifs forming the A-site are far apart from each other, as long as the site is not occupied (Figure 2A). This long distance had strengthened the initial interpretation that these two motifs form the binding sites of the two substrates, respectively (*35*). A slight induced fit is also observed on I-site binding. It involves conformational changes of the side-chains of Lys112 and Arg163 and also a flip of the peptide bond 109−110.

CONCLUSION

By providing the structure of the reaction product bound to a member of the FPP synthase family, we were able to deduce the reaction geometry in fine detail. This geometry fits the known chemical data in all respects, requiring only minor atom movements during the reaction. We have emphasized the intrinsic difference of the two involved diphosphate sites and outlined the induced fit occurring on substrate binding to the A- and I-sites.

ACKNOWLEDGMENT

We thank the team of the Swiss Light Source in Villigen (Switzerland) for their support.

REFERENCES

1. Sacchettini, J. C., and Poulter, C. D. (1997) Creating isoprenoid diversity. *Science 277*, 1788−1789.
2. Rüdiger, W., Benz, J., and Guthoff, C. (1980) Detection and partial characterization of activity of chlorophyll synthetase in etioplast membranes. *Eur. J. Biochem. 109*, 193−200.
3. Olszewski, N., Sun, T., and Gubler, F. (2002) Gibberelin signaling: biosynthesis, catabolism, and response pathways. *Plant Cell 14*, Supplemental Information S61−80.
4. Harris, C. M., and Poulter, C. D. (2000) Recent studies of the mechanism of protein prenylation. *Nat. Prod. Rep. 17*, 137−144.
5. Kloer, D. P., and Schulz, G. E. (2006) Structural and biological aspects of carotenoid cleavage. *Cell. Mol. Life Sci.*, in press, DOI 10.1007/s00018-006-6176-6.
6. Goldstein, J. L., and Brown, M. S. (1990) Regulation of the mevalonate pathway. *Nature 343*, 425−430.
7. Eisenreich, W., Bacher, A., Arigoni, D., and Rohdich, F. (2004) Biosynthesis of isoprenoids via the non-mevalonate pathway. *Cell. Mol. Life Sci. 61*, 1401−1426.
8. Ogura, K., and Koyama, T. (1998) Enzymatic aspects of isoprenoid chain elongation. *Chem. Rev. 98*, 1263−1276.
9. Ohnuma, S., Koyama, T., and Ogura, K. (1991) Purification of solanesyl−diphosphate synthase from *Micrococcus luteus.* A new class of prenyltransferase. *J. Biol. Chem. 266*, 23706−23713.
10. Fujihashi, M., Zhang, Y. W., Higuchi, Y., Li, X. Y., Koyama, T., and Miki, K. (2001) Crystal structure of *cis*-prenyl chain elongating enzyme, undecaprenyl diphosphate synthase. *Proc. Natl. Acad. Sci. U.S.A. 98*, 4337−4342.
11. Guo, R. T., Ko, T. P., Chen, A. P. C., Kuo, C. J., Wang, A. H. J., and Liang, P. H. (2005) Crystal structures of undecaprenyl pyrophosphate synthase in complex with magnesium, isopentenyl pyrophosphate, and farnesyl thiopyrophosphate. Roles of the metal ion and conserved residues in catalysis. *J. Biol. Chem. 280*, 20762−20774.
12. Wang, K. C., and Ohnuma, S. (2000) Isoprenyl diphosphate synthases. *Biochim. Biophys. Acta 1529*, 33−48.
13. Tarshis, L. C., Yan, M., Poulter, C. D., and Sacchettini, J. C. (1994) Crystal structure of recombinant farnesyl diphosphate synthase at 2.6 Å resolution. *Biochemistry 33*, 10871−10877.
14. Sun, H. Y., Ko, T. P., Kuo, C. J., Guo, R. T., Chou, C. C., Liang, P. H., and Wang, A. H. J. (2005) Homodimeric hexaprenyl pyrophosphate synthase from the thermoacidophilic crenarchaeon *Sulfolobus solfataricus* displays asymmetric subunit structures. *J. Bacteriol. 187*, 8137−8148.
15. Guo, R. T., Kuo, C. J., Chou, C. C., Ko, T. P., Shr, H. L., Liang, P. H., and Wang, A. H. J. (2004) Crystal structure of octaprenyl pyrophosphate synthase from hyperthermophilic *Thermotoga maritima* and mechanism of product chain length determination. *J. Biol. Chem. 279*, 4903−4912.
16. Kavanagh, K. L., Dunford, J. E., Bunkoczi, G., Russell, R. G. G., and Oppermann, U. (2006) The crystal structure of human geranylgeranyl pyrophosphate synthase reveals a novel hexameric arrangement and inhibitory product binding. *J. Biol. Chem. 281*, 22004−22012.
17. Yoshida, I., Koyama, T., and Ogura, K. (1989) Formation of a stable and catalytically active complex of the two essential components of hexaprenyl diphosphate synthase from *Micrococcus luteus* B-P 26. *Biochem. Biophys. Res. Commun. 160*, 448−452.
18. Bonk, M., Hoffmann, B., von Lintig, J., Schledz, M., Al-Babili, S., Hobeika, E., Kleinig, H., and Beyer, P. (1997) Chloroplast import of four carotenoid biosynthetic enzymes *in vitro* reveals differential fates prior to membrane binding and oligomeric assembly. *Eur. J. Biochem. 247*, 942−950.
19. Doublie, S. (1997) Preparation of seleno−methionyl proteins for phase determination. *Methods Enzymol. 276*, 523−530.
20. Kabsch, W. (1993) Automatic processing of rotation diffraction data from crystals of initially unknown symmetry and cell constants. *J. Appl. Crystallogr. 26*, 795−800.
21. Schneider, T. R., and Sheldrick, G. M. (2002) Substructure solution with SHELXD. *Acta Crystallogr. B24*, 63−76.
22. de la Fortelle, E., and Bricogne, G. (1997) Maximum-likelihood heavy-atom parameter refinement for multiple isomorphous replacement and multiwavelength anomalous diffraction methods. *Methods Enzymol. 276*, 472−494.
23. Terwilliger, T. C. (2000) Maximum likelihood density modification. *Acta Crystallogr. D57*, 965−972.
24. Perrakis, A., Morris, R., and Lamzin, V. S. (1999) Automated protein model building combined with iterative structure refinement. *Nat. Struct. Biol. 6*, 458−463.
25. McRee, D. E. (1999) XtalView/Xfit−A versatile program for manipulating atomic coordinates and electron density. *J. Struct. Biol. 125*, 156−165.
26. Tronrud, D. E., Ten Eyck, L. F., and Matthews, B. W. (1987) An efficient general-purpose least-squares refinement program for macromolecular structures. *Acta Crystallogr. A43*, 489−501.
27. Roversi, P., Blanc, E., Vonrhein, C., Evans, G., and Bricogne, G. (2000) Modeling prior distributions of atoms for macromolecular refinement and completion. *Acta Crystallogr. D56*, 1313−1323.
28. Murshudov, G. N., Vagin, A. A., and Dodson, E. J. (1997) Refinement of macromolecular structures by the maximum-likelihood method. *Acta Crystallogr. D53*, 240−255.
29. Schüttelkopf, A. W., and von Aalten, D. M. F. (2004) PRODRG: a tool for high-throughput crystallography of protein−ligand complexes. *Acta Crystallogr. D60*, 1355−1363.
30. Jelakovic, S., and Schulz, G. E. (2002) Catalytic mechanism of CMP: 2-keto-3-deoxy-*manno*-octonic acid synthetase as derived from complexes with reaction educt and product. *Biochemistry 41*, 1174−1181.
31. Blom, N., and Sygusch, J. (1997) Product binding and role of the C-terminal region in class I D-fructose 1, 6-bisphosphate aldolase. *Nat. Struct. Biol. 4*, 36−29.
32. Joerger, A. C., Mueller-Dieckmann, C., and Schulz, G. E. (2000) Structures of L-fuculose-1-phosphate aldolase mutants outlining motions during catalysis. *J. Mol. Biol. 303*, 531−543.
33. Hosfield, D. J., Zhang, Y., Dougan, D. R., Broun, A., Tari, L. W., Swanson, R. V., and Finn, J. (2004) Structural basis for bisphosphonate-mediated inhibition of isoprenoid biosynthesis. *J. Biol. Chem. 279*, 8526−8529.
34. Holm, L., and Sander, C. (1993) Protein structure comparison by alignment of distance matrices. *J. Mol. Biol. 233*, 123−138.
35. Tarshis, L. C., Proteau, P. J., Kellogg, B. A., Sacchettini, J. C., and Poulter, C. D. (1996) Regulation of product chain length by isoprenyl diphosphate synthases. *Proc. Natl. Acad. Sci. U.S.A. 93*, 15018−15023.
36. Chang, T. H., Guo, R. T., Ko, T. P., Wang, A. H. J., and Liang, P. H. (2006) Crystal structure of type-III geranylgeranyl pyrophosphate synthase from *Saccharomyces cerevisiae* and the mechanism of product chain length determination. *J. Biol. Chem. 281*, 14991−15000.
37. Caruthers, J. M., Kang, I., Rynkiewicz, M. J., Cane, D. E., and Christianson, D. W. (2000) Crystal structure determination of aristolochene synthase from the blue cheese mold *Penicillium roqueforti. J. Biol. Chem. 275*, 25533−25539.
38. Pandit, J., Danley, D. E., Schulte, G. K., Mazzalupo, S., Pauly, T. A., Hayward, C. M., Hamanaka, E. S., Thompson, J. F., and Harwood, H. J., Jr. (2000) Crystal structure of human squalene synthase. *J. Biol. Chem. 275*, 30610−30617.
39. Kavanagh, K. L., Guo, K., Dunford, J. E., Wu, X., Knapp, S., Ebetino, F. H., Rogers, M. J., Russell, R. G. G., and Oppermann, U. (2006) The molecular mechanism of nitrogen-containing bisphosphonates as anti-osteoporosis drugs. *Proc. Natl. Acad. Sci. U.S.A. 103*, 7829−7834.
40. Rondeau, J. M., Bitsch, F., Bourgier, E., Geiser, M., Hemmig, R., Kroemer, M., Lehmann, S., Ramage, P., Rieffel, S., Strauss,

A., Green, J. R., and Jahnke, W. (2006) Structural basis for the exceptional *in vivo* efficacy of bisphosphonate drugs. *ChemMedChem 1*, 267−273.

41. Cornforth, J. W., Cornforth, R. H., Popjak, G., and Yengoyan, L. (1966) Studies on the biosynthesis of cholesterol XX. Steric course of decarboxylation of 5-pyrophosphomevalonate and of the carbon to carbon bond formation in the biosynthesis of farnesyl pyrophosphate. *J. Biol. Chem. 241*, 3970−3987.
42. Gabelli, S. B., McLellan, J. S., Montalvetti, A., Oldfield, E., Docampo, R., and Amzel, L. M. (2006) Structure and mechanism of the farnesyl diphosphate synthase from *Trypanosoma cruzi*: Implications for drug design. *Proteins: Struct., Funct., Bioinform. 62*, 80−88.

BI061572K